Atmospheric Environment 48 (2012) 76–84

Contents lists available at ScienceDirect

Atmospheric Environment

journal homepage: www.elsevier.com/locate/atmosenv

Volcanic aerosol optical properties and phase partitioning behavior after long-range advection characterized by UV-Lidar measurements

A. Miffre [a,*], G. David [a], B. Thomas [a], P. Rairoux [a], A.M. Fjaeraa [b], N.I. Kristiansen [b], A. Stohl [b]

[a] Laboratoire de Spectrométrie Ionique et Moléculaire, CNRS UMR 5579 Université Lyon 1, 10 rue Ada Byron, 69622 Villeurbanne, France
[b] Norwegian Institute for Air Research (NILU), N-2027 Kjeller, Norway

ARTICLE INFO

Article history:
Received 8 December 2010
Received in revised form
23 March 2011
Accepted 25 March 2011

Keywords:
Volcanic ash
Lidar
Depolarization
Dispersion model

ABSTRACT

In this paper, an UV-polarization Lidar is used to study the optical properties of volcanic aerosol in the troposphere. The particles were released by the mid-April 2010 eruption of the Eyjafjallajökull volcano (63.63°N, 19.62°W, Iceland) and passed in the troposphere above Lyon (45.76°N, 4.83°E, France) after advection over 2600 km. The FLEXPART particle dispersion model was applied to simulate the volcanic ash transport from Iceland to South West Europe, at the border of the air traffic closure area. Time-altitude plots of FLEXPART ash concentrations as well as of aerosol backscattering are presented, showing the arrival of volcanic particles in the troposphere above Lyon and their mixing into the planetary boundary layer. The particle UV-backscattering coefficient was typically 4 Mm^{-1} sr^{-1} and highly sensitive and accurate particle UV-depolarization measurements were performed, with depolarization ranging from a few to 44%. After few days long-range transport, observed ash particles are still non spherical. The observed variations of the backscattering and depolarization coefficients can be attributed to variations in the volcanic particles content. Ash mass concentrations are then retrieved. Moreover, a partitioning into spherical and non spherical particles is evaluated from number concentration ratios between solid ash particles and spherical hydrated sulfate particles. The microphysical properties of volcanic particles can thus be studied by associating an UV-polarization remote sensing instrument with a numerical volcanic ash dispersion model.

1. Introduction

Volcanic eruptions release particles and gases such as sulfur dioxide (SO_2) into the atmosphere that have implications on global climate. For example, Pinatubo's eruption in 1991 injected large quantities of SO_2 into the stratosphere, which caused an anomalous cooling of the Earth's surface (Ramaswamy et al., 2001). Volcanic aerosols emitted to the troposphere affect climate through both direct and indirect effects, however this topic is still subject to large uncertainties (Robock, 2000). The physical and chemical properties of volcanic particles are modified during advection, especially in the troposphere where the chemical processing is fast. During their transport, irregularly-shaped volcanic ash particles such as silica glass or feldspar crystals with sizes larger than about 20 μm diameter are rapidly removed from the volcanic cloud by gravitational settling. In contrast, finer ash particles and secondary aerosols such as hydrated sulfates, formed by SO_2-oxidation, may remain in the troposphere for several weeks (Ovadnevaite et al., 2009).

After advection over several thousands of kilometers, the volcanic ash particles are highly dispersed and aged. When they reach the lower troposphere, they are especially interesting to study for at least two reasons: firstly, their microphysical properties, such as shape and size, which have been changing during advection, are not well known, as measurements are rather seldom and focus on the particles size distribution (Schumann et al., 2010). Secondly, in the absence of precipitation, the particle residence time in the free troposphere can be much longer than the typical residence time of anthropogenic particles in the planetary boundary layer (PBL), amplifying their impacts on the regional radiation budget (Robock, 2000). To study the transport of volcanic particles in the atmosphere, a wide range of atmospheric dispersion models is available (Witham et al., 2007). These atmospheric dispersion numerical models, running at a continental scale, are typically validated using local ground-based or satellite-based remote sensing instruments (Eckhardt et al., 2008). Mt Etna's eruption in the year 2002 has recently been studied by Wang et al. (2008) in this way. Hence, the physical and chemical transformations of the ash-loaded volcanic

* Corresponding author. Tel.: +33 472 431 087; fax: +33 472 431 507.
E-mail address: miffre@lasim.univ-lyon1.fr (A. Miffre).

1352-2310/$ – see front matter © 2011 Elsevier Ltd. All rights reserved.
doi:10.1016/j.atmosenv.2011.03.057

cloud can be evaluated during its dispersion. Moreover, information on the shape of the volcanic particles can be gathered by Lidar (Light-Detection-And-Ranging) measurements of the volcanic particles' ability to depolarize laser light. This is well-established in stratospheric research (Winker and Osborn, 1992). In the troposphere, such depolarization measurements are also performed in the visible spectral range (Murayama et al., 2003), but are rather seldom for volcanic aerosols. Sassen et al. (2007) reported such depolarization measurements, showing the irregular shape of particles remaining after advection over a few hundred of kilometers from an Alaskan volcano.

The Eyjafjallajökull volcano (63.63°N, 19.62°W, Iceland), hereafter named Eyjafjalla, started to erupt on March 20th 2010, before entering an explosive phase on April 14th 2010 lasting for several days, followed by further explosive eruptions during May 2010. In the initial explosive phase in April 2010, the eruption ejected volcanic ash to altitudes as high as 9 km above sea level (ASL), as reported by the Institute of Earth Sciences (IES, http://www.earthice.hi.is). On April 15th and 16th, the volcanic activity and ash generation continued, with reduced activity from April 16th. IES chemical analyses of ash samples revealed eruptive products with a silica content of 58% by weight, alumina Al_2O_3 (15%), and oxides (FeO, CaO, <10%). SO_2 fluxes of 3 kt day^{-1} were reported by the Icelandic METOffice (http://en.vedur.is/), comparable with the annual flux of SO_2 normally emitted by the whole Icelandic volcanic region (Halmer et al., 2002). As shown by MODerate resolution Imaging Spectrometer MODIS (http://modis.gsfc.nasa.gov/) on April 15th, the volcanic cloud emitted by the strong initial eruption on 14th April was transported eastwards and subsequently spread over northern Europe before reaching the South of France, leading to a six-days closure of the airspace for aviation over western Europe due to possible hazards to aircraft (Prata and Tupper, 2009).

In this contribution, we focus on the optical properties of the volcanic particles that were released by the mid-April 2010 eruption of the Eyjafjalla volcano and passed in the troposphere above Lyon (45.76°N, 4.83°E, France), after advection over more than 2600 km. Lyon is located in the Rhône valley and during the Eyjafjalla eruption, Lyon was at the border of the air traffic closure area (cities located further to the South had no airport closure) and thus the volcanic particles reaching Lyon were highly diluted. In this paper, an analysis of the optical properties of the Eyjafjalla volcanic ash cloud is performed by combining UV-polarization measurements done with a sensitive tropospheric Lidar instrument and results from the FLEXPART particle dispersion model. The Lidar instrument used is described in Section 2. The volcanic particles optical properties are then presented in Section 3, where UV-backscattering coefficients and UV-depolarization ratios are retrieved from our Lidar measurements, to address the amount of spherical and non spherical particles in the volcanic ash cloud. These optical properties are then analyzed in Section 4 where the agreement between the Lidar-observed air masses and FLEXPART simulated ash layers is discussed. Our highly sensitive and precise UV-depolarization measurements allowed us to identify different volcanic layers with different depolarization ratios, ranging from a few to 44%, in remarkable agreement with laboratory measurements (Munoz et al., 2004). These varying depolarization ratios can be interpreted by variations in the ash concentration number and by assuming hygroscopic growth of sulfate particles (Allen et al., 2002). Furthermore, an optical scattering computation of the ash-loaded volcanic cloud was made to derive the ratio between the concentration number of spherical particles (hydrated sulfates) and non spherical particles (ash). We believe such a partitioning between spherical and non spherical particles, derived from both scattering and depolarization processes, to be relevant for further understanding the particle microphysics involved in volcanic clouds.

2. Methodology

2.1. Meteorological conditions

Between 17th and 20th of April 2010, the weather conditions over Lyon were determined by a high-pressure system located over France. This allowed us to perform Lidar measurements continuously and follow the evolution of volcanic ash layers over the Lidar site, except during a short rain episode that occurred in the evening on April 18th. Vertical profiles of temperature (temperature T, dew point temperature T_d, potential temperature θ) and relative humidity (RH) are displayed in Fig. 1 for several selected times. These profiles were taken from meteorological analyses of the European Center for Medium-Range Weather Forecasts (ECMWF) and are in good agreement with radiosonde balloon measurements performed at the local Bron Météo-France station. Over the whole measurement period, dew point temperatures were always lower than observed temperatures. The potential temperature shows an inversion layer at 1.5 km on April 17th at 12 h UTC (profile (a)) and at 2.5 km on April 19th at 0 UTC (profile (b)). Above this altitude, where volcanic layers were observed, the troposphere is stably stratified. Close to the ground, RH ranges between 50 and 75%, and it reaches 70% near 3 km altitude. However, the volcanic aerosol layers observed around 4–5 km experienced very low (10–25%) RH-values. These meteorological data will be further analyzed in the next sections together with the depolarization measurements.

2.2. Lidar experimental set-up

The Lidar consists of a linear polarized 10-Hz repetition rate Nd:YAG laser emitting at 355 nm wavelength, combined with a 200 mm Newtonian telescope to collect backscattered light from atmospheric particles (p) and molecules (m). Backscatter of UV-light is sensitive to both fine (diameter $d < 0.5$ μm) and coarse (higher d-values) mode particles (Mishchenko, 2002). Two successive polarizing beam-splitter cubes (PBC) separate parallel ($P_{//}$) and cross-polarized ($P_{\perp}$) Lidar return elastic signals with respect to the laser polarization plane to measure the depolarization ratio $P_{\perp}/P_{//}$. Use of a secondary PBC ensures the polarization purity of both detection channels and, thus, that the cross-talk between the channels is negligible with an accuracy better than 10^{-7}. The amount of Raman rotational sidebands that contribute to the strong UV-molecular scattering is minimized by using a very selective interference filter ($\Delta\lambda = 0.35$ nm), which also reduces sky background contribution. Depolarization ratio measurements have been performed at three times, labeled from (a) to (c) in the figures. Each Lidar acquisition is time-averaged over 7 min and repeated every 20 min. The recorded Lidar signal is sampled with a 12-bits 40-MHz Licel AD-converter. High-frequency noise filtering and range averaging lead to a final vertical resolution of 75 m. Lidar backscattering measurements have been performed between 0.6 and 6 km-altitude ASL, limited close to the ground, by an incomplete emitter/receiver overlap function. This systematic error does not affect the observation of the volcanic cloud, whose layers were mostly found above 2 km ASL. We limited our particle UV-depolarization ratio measurements to 5 km altitude ASL in order to retain a high signal-to-noise range ratio of better than 3.

2.3. Calculation of volcanic particles optical properties

To help interpret the scattering and depolarization Lidar measurements in terms of particle mass concentrations (see Section 4), the volcanic cloud optical scattering properties have been computed. Volcanic particles are assumed to be composed of ash particles and hygroscopic sulfates (Mather et al., 2003;

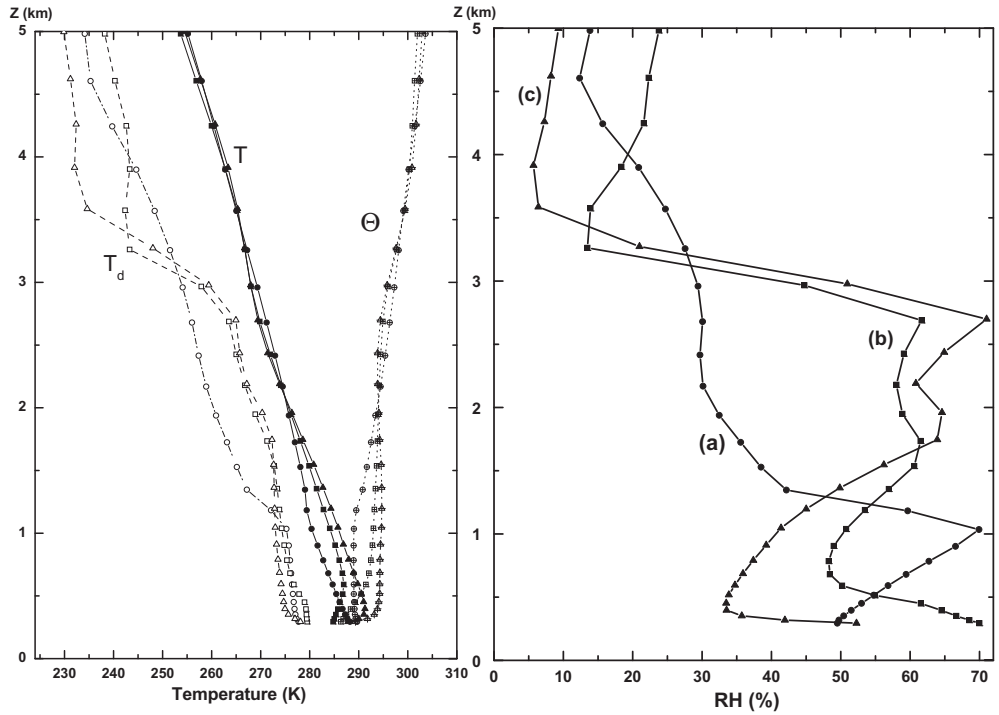

Fig. 1. Vertical profiles of dew point temperature (T_d, left part, empty sign), temperature (T, middle part, full sign), potential temperature (θ, right part, cross sign) and relative humidity (RH) supplied by the European Center for Medium-Range Weather Forecasts (ECMWF) for Lyon for specific times analyzed with the depolarization measurement (Section 3.2): (a) April 17th at 12 h UTC (circles), (b) April 19th at 0 h UTC (squares), (c) April 19th at 19 h UTC (triangles).

Schumann et al., 2010). Ammonium sulfates and other compounds have not been considered as time-delays larger than two days are needed to neutralize sulfates (Mather et al., 2003). For computing the backscattering of ash particles, instead of applying T-matrix formalism for randomly oriented particles, scattering phase function, refractive index at 355 nm and ash size distribution have been taken from the analysis by Munoz et al. (2004) of Mt. Spurr's eruption, which produced a similar particle composition as the Eyjafjalla eruption. Particles with diameters larger than 20 μm are not considered in the calculation as the FLEXPART simulation (see Section 2.5) suggested that these particles were largely lost by settling before reaching Lyon. By using scattering matrix formalism (Mishchenko, 2002), we derived for both polarizations size-weighted particle backscattering differential cross-sections for ash particles. For spherical particles, assumed to be mainly sulfates, Mie optical scattering has been applied, with a double log normal distribution and water uptake coefficient taken from Li et al. (2001), to derive size-weighted particle backscattering cross-sections for spherical particles. Table 1 summarizes the size distribution parameters and refractive index values used.

Moreover, from Munoz's laboratory measurements on randomly oriented ash particles, we derived optical scattering matrix elements (F_{ij}) in the backscattering case, independent of the wavelength in the UV–VIS spectral range. We thus deduce the depolarization ratio of volcanic ash particles: $\delta_p(\text{ash}) = (1 - F_{22}/F_{11})/(1 + F_{22}/F_{11}) = 44\%$, which results from the sharp edges and the highly irregular shape of ash particles, mostly composed of silicate, glass and mineral.

2.4. FLEXTRA air masses back-trajectories

We evaluate the origin of the air passing above the UV-polarization Lidar station by computing 7-days air parcels back-trajectories, with 6 h resolution, using the trajectory model FLEXTRA (Stohl et al., 1995). The model employs wind fields from the ECMWF at a latitude/longitude resolution of 1° × 1° and at 91 pressure levels. Fig. 2 presents the analytical back-trajectories, which show the history of the air parcels arriving at Lyon, for altitudes between 3 and 5 km from April 17th to 19th. It indicates that for a range of altitudes in the lower free troposphere, trajectories reaching the Lidar location between 17th and 19th of April had traveled across southern Iceland two or three days earlier. According to these back-trajectories, Saharan dust can be excluded as a source of particles over Lyon during the observation period.

2.5. FLEXPART particle dispersion model

We also performed simulations with the Lagrangian particle dispersion model FLEXPART (Stohl et al., 2005; Eckhardt et al., 2008), driven with ECMWF data with 0.18° × 0.18° resolution in the area of interest (1° × 1° globally). FLEXPART simulates the advection by the large-scale winds, as well as turbulence and

Table 1
Size distribution parameters (radius r, geometrical mean σ, relative concentration N), refractive index for computation of backscattering cross-sections for ash and sulfates particles.

Particles	Bimodal size distribution						Refractive index at 355 nm (m)
	r_1 (μm)	σ_1 (μm)	N_1 (cm^{-3})	r_2 (μm)	σ_2 (μm)	N_2 (cm^{-3})	
Ash	0.15	2.8	1	4	2.5	5.0×10^{-3}	$1.52 + 6 \times 10^{-3}$i (Munoz et al., 2004)
Sulfates	0.01	2.2	1	0.15	2.2	1.0×10^{-3}	$1.42 + 6 \times 10^{-3}$i (Krotkov et al., 1997)

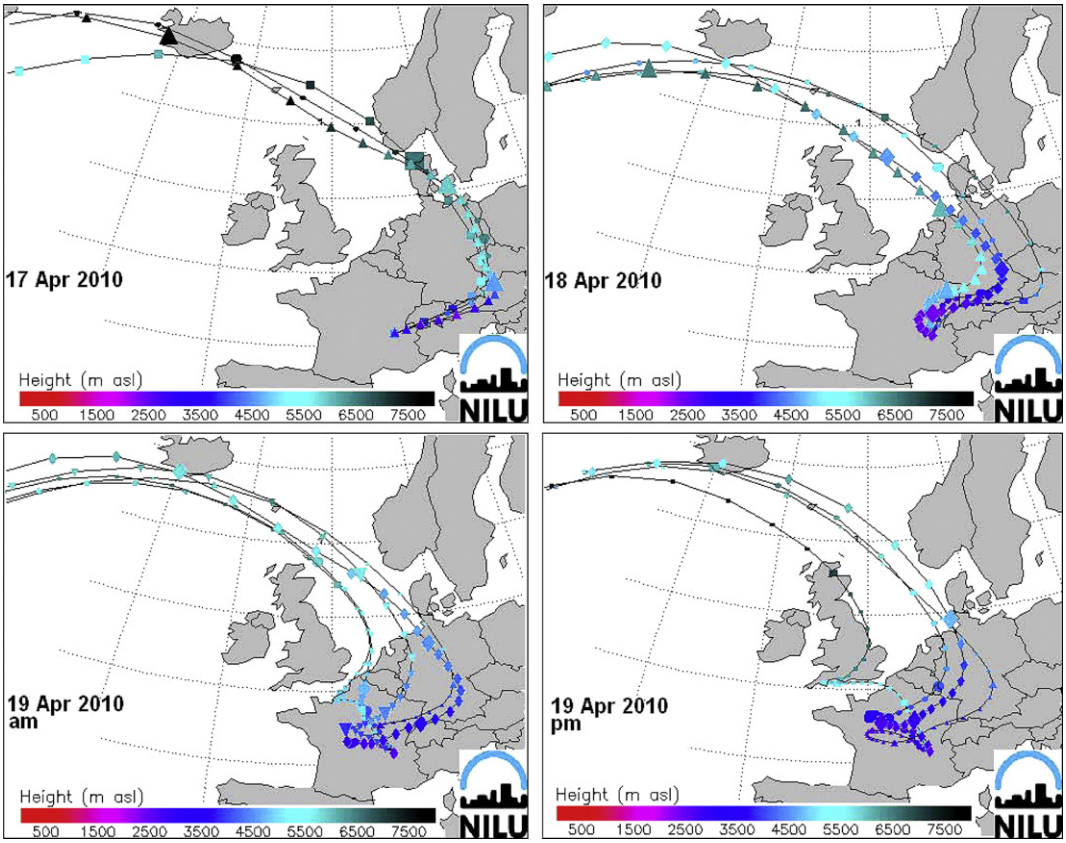

Fig. 2. Back-trajectories at Lyon at different altitudes for different times. Upper left graph: April 17th at 6 h (5 km, circles (c)), 12 h (5 km, squares (s)), 18 h (4 km, triangles (t)). Upper right graph: April 18th at 12h (4 km, c) and (5 km, s), at 18h (3 km, diamonds (d)) and (5 km, t). Lower left graph: April 19th at 0 h (3 km, low t), (4 km, c), (5 km, s); at 6 h (3 km,d) and (4 km, upper t). Lower right graph: April 19th at 12 h (3 km, d), at 18h (2 km, t), (3 km, c), (5 km, s).

convection. Sedimentation, dry and wet deposition of the particles were considered in the simulation (Stohl et al., 2005). The ash source strength was determined by an inversion algorithm, which will be described elsewhere (Stohl et al., 2011). 21 million particles were released from the volcano and were binned in 25 particle size classes, between 0.25 and 250 μm diameter. The largest ash particles mostly fall out by gravitational settling during the 48 h-advection time to Lyon, leaving fine ash particles with sizes up to about 20 μm diameter at the Lidar location in the simulation. Ash particles, which dominate the aerosol mass are taken into account but the formation of sulfate particles is not simulated by FLEXPART. However, their transport should be relatively similar to the smallest simulated ash particles. The volcanic ash distribution over Europe on April 17th at 12 h UTC as simulated by FLEXPART is presented in Fig. 3 showing that ash particles arriving at Lyon were highly dispersed, even already on April 17th. The simulated vertical distribution of the volcanic ash above Lyon between 17th and 20th April is shown on top of Fig. 4, where we can clearly see a thin simulated ash layer tilting from 6 km ASL at 0 h UTC on 17 April to 4 km ASL 12 h later, where it remains until 6 h UTC on 18 April. Later on 18 April, the ash is mixed down into the PBL and distributed throughout the lowest 4 km for the rest of the observation period.

3. Optical properties of volcanic aerosols

3.1. Particle UV-backscattering coefficient β_p

We have measured the particle UV-backscattering coefficient β_p, which is proportional to the particle number concentration and also depends on particle size, shape and chemical composition. β_p is determined from the scattering ratio R, defined as the ratio between total (p, m) and molecular (m) backscattering coefficients:

$$\beta_p = (R-1)\beta_m \quad (1)$$

R is equal to unity for a particle-free atmosphere and the Klett's algorithm (1985) was used to retrieve R as a function of altitude (Böckmann et al., 2005). To apply the Klett inversion, a predefined value of the extinction-to-backscatter ratio S is needed (S is the ratio between particle extinction coefficient α_p and particle backscattering coefficient β_p). S is not exactly known since it is range-dependent, sensitive to the particles' microphysics and chemical composition (Ackermann, 1998). In this study, we assumed a constant S-ratio of (55 ± 5) sr, in agreement with recent measurements performed during the mid-April Eyjafjalla eruption (Ansmann et al., 2010) and with older tropospheric measurements for Etna's eruption in 2002 (Wang et al., 2008). The accuracy on

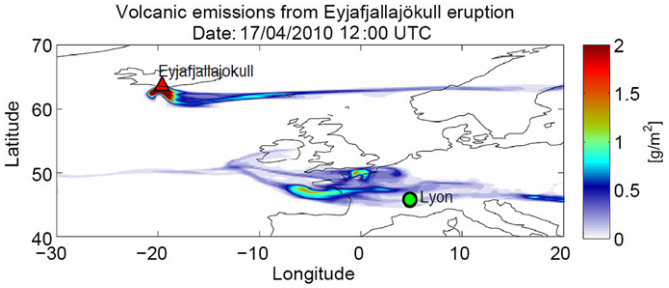

Fig. 3. FLEXPART ash tracer simulation of the volcanic cloud emitted during the mid-April Eyjafjalla volcano eruption at Lyon on April 17th at 12 h.

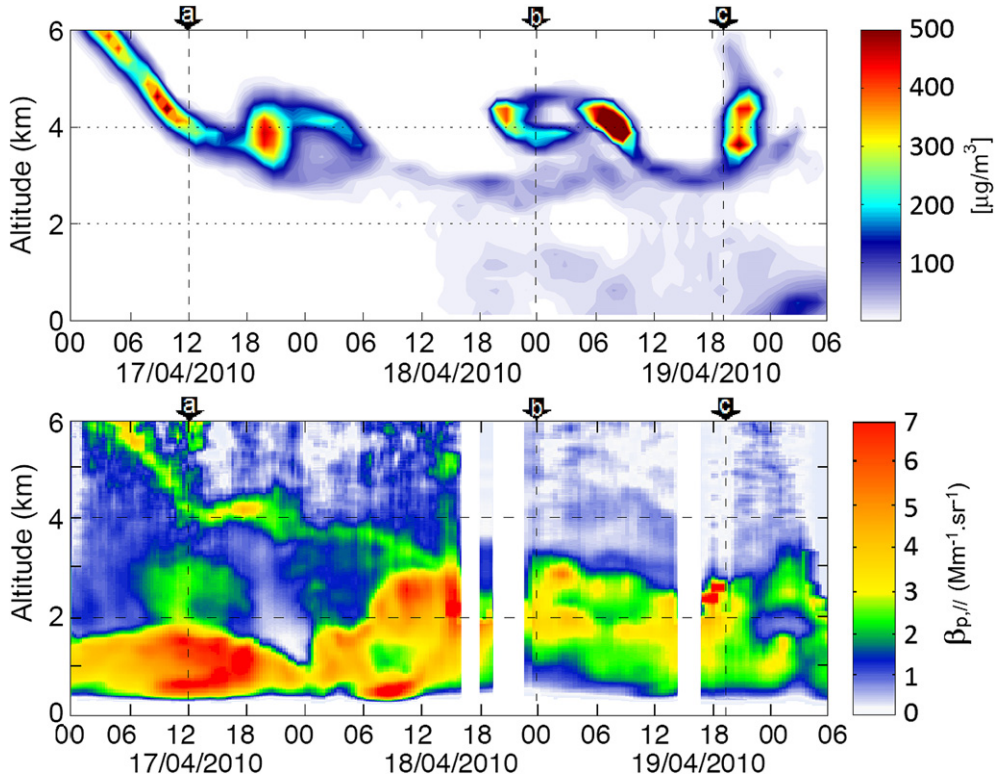

Fig. 4. Top graph: FLEXPART time-height section of the ash tracer at Lyon. Bottom graph: Parallel UV-particle backscattering coefficient (in Mm^{-1} sr^{-1}) at Lyon as a function of time (in UTC units) from April 17th to 20th 2010. Letters from (a) to (c) correspond to depolarization profile's times, to be analyzed in Section 4.

retrieved *R*-values is determined at altitude z from the maximum difference obtained when using the maximum and minimum values of *S*. Above 2 and up to 6 km ASL, *R*-values are known with an uncertainty of less than 10%. By applying this procedure to the parallel polarization channel, we retrieved the particle volume backscattering coefficient $\beta_{p,//}$as a function of altitude for the whole measurement period.

Vertical profiles of $\beta_{p,//}$are displayed in Fig. 4 (bottom) as a function of time from April 17th to 20th. The white-colored areas correspond to short rain episodes which prevented the evaluation of backscattering coefficients. Largest $\beta_{p,//}$-values occur near the ground where the particle load is largely dominated by local emissions of aerosols (and their precursors) (Miffre et al., 2010). An enhancement of backscattering is visible on April 18th from two to 3 km, that can be related to FLEXPART simulation. Between 3 and 6 km, an unusually high particle load is visible on April 17th and 18th in a thin filament, with $\beta_{p,//}$-values between 2 and 5 Mm^{-1} sr^{-1}. The filament tilts from 6 km to 4 km on April 17th at 12 h, and then at 3 km on April 18th in the evening before mixing into the PBL. On April 19th, measured particle backscattering coefficients are lower because of less direct atmospheric transport and decreased volcanic activity (Schumann et al., 2010): $\beta_{p,//}$-values do not exceed 3.5 Mm^{-1} sr^{-1}, except for the 3 km altitude cloud seen on April 19th at 18 h.

3.2. Particle UV-depolarization δ_p

After advection over more than 2600 km, the highly dispersed and aged volcanic particles passing above the Lidar station may have a different shape from their initial shape. In particular sulfate particles will have formed from the sulfur dioxide emitted along with the volcanic ash. Particles having a non spherical shape depolarize laser light and the magnitude of this depolarization can be remotely measured with the range-resolved perpendicular Lidar channel. Hence, the particles' ability to depolarize laser light is mainly governed by their shape (Mishchenko, 2002). We have measured the particle linear volume UV-depolarization ratio $\delta_p = \beta_{p,\perp}/\beta_{p,//}$, defined as the ratio between perpendicular and parallel particle backscattering coefficients. δ_p is retrieved from the total depolarization δ and its molecular contribution δ_m (Winker and Osborn, 1992):

$$\delta_p = \frac{R_{//}\delta - \delta_m}{R_{//} - 1} \quad (2)$$

where the parallel Lidar ratio $R_{//} = 1 + \beta_{p,//}/\beta_{m,//}$ has been used in section 3.1 to derive the parallel particle backscattering coefficient $\beta_{p,//}$. To discriminate between different depolarizing volcanic particles layers, it is necessary to precisely determine δ_p. Special care has been taken to minimize the different systematic errors contributing to δ_p. The spectral selectivity of our detector determines the molecular depolarization $\delta_m = 3.7 \times 10^{-3}$. The total depolarization δ is deduced from the measured depolarization ratio $\delta^* = P_\perp/P_{//}$ by performing a very accurate calibration procedure to determine the electro-optics calibration constant $G = \delta^*/\delta$ directly at studied altitudes, using Alvarez's et al. (2006), based on rotating a half-wave plate to introduce controlled amounts of polarization cross-talks. The accuracy of δ-values is determined by the 2%-uncertainty of G ($G = 16.2 \pm 0.3$) and the range-dependent uncertainty on δ^*, reduced by time and range averaging. An example of a vertical profile of δ_p values is given in Fig. 5, for April 17th at 12 h, together with the corresponding backscattering coefficients and the total depolarization δ. Largest δ_p-values correlate with largest δ-values. Despite strong UV-molecular scattering, $\beta_{p,\perp}$ lies in the range of tenths of $\beta_{p,//}$, and δ_p-values are

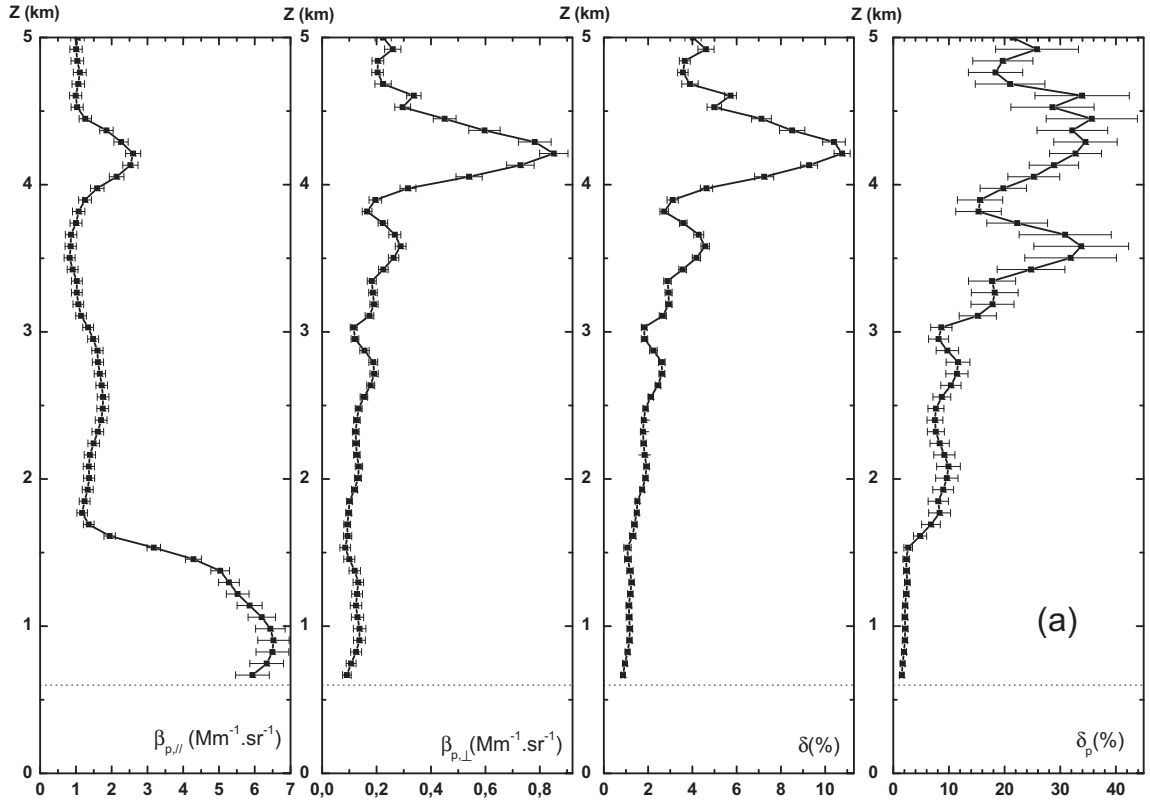

Fig. 5. Vertical profiles of parallel and perpendicular particle UV-backscattering coefficients $\beta_{p,//}$, $\beta_{p,\perp}$, total UV-depolarization δ and particle UV-depolarization ratio δ_p on April 17th at 12 h UTC (profile (a)). The error bars on δ_p have been calculated using equation (3).

known with a high sensitivity, from a few to several tens of %. Moreover, the uncertainty on δ_p, determined by using equation (2),

$$\frac{\Delta\delta_p}{\delta_p} = \frac{R_{//}\Delta\delta}{R_{//}\delta - \delta_m} + \frac{\delta\Delta R_{//}}{R_{//}\delta - \delta_m} + \frac{\Delta R_{//}}{R_{//} - 1} \quad (3)$$

is below 30%, for altitudes lower than 5 km ASL, and largely dominated by the 10%-uncertainty on the assumed extinction-to-backscatter S-ratio. Following the same procedure, vertical profiles of δ_p have been obtained also for two selected times on April 19th; profiles are displayed in Fig. 6.

4. Results and discussion

4.1. Comparison between observed aerosol layers and FLEXPART simulated ash layers

The Lidar-observed filament structure (bottom of Fig. 4) nicely agrees with the FLEXPART simulated ash layers (top of Fig. 4) within the vertical and time resolutions of both methodologies. We clearly see its tilting into the low troposphere on April 17th in the early morning from initially 6 km to about 4 km around midday. Agreement is observed even for some small-scales features, for instance the maximum on April 17th at 18 h at 4 km. The comparison between the simulated and observed ash layers relies on the proportionality between $\beta_{p,//}$ and the particles' number concentration and furthermore to the mass concentration (Miffre et al., 2010). Correlation with FLEXTRA back-trajectories confirms the volcanic origin of the air masses passing above the Lidar site. Hence, the volcanic cloud optical properties can be analyzed with our Lidar instrument in these specific layers. The filament structure suggests that the ash layers remained highly stratified even after long-range advection. On April 17th, the observed layers below the filament (2–3 km) correspond to air masses originating from the East of Europe and are, thus, of non-volcanic origin. We evaluated the particle backscattering coefficient $\beta_p = \beta_{p,//} + \beta_{p,\perp}$ of the volcanic layer, on the specified time to :

$$\beta_p(\text{UV, April 17th, 12 h UTC, 4.2 km}) = (3.4 \pm 0.3)\ \text{Mm}^{-1}\ \text{sr}^{-1} \quad (4)$$

leading to an integral backscattering coefficient for volcanic particles of 2×10^{-3} sr^{-1}. Using $S = (55 \pm 5)$ sr, the UV-particle extinction coefficient is $\alpha_p = (187 \pm 34)$ Mm^{-1}. Using ash simulated backscattering cross-sections (see Section 2.3) and $\beta_{p,\perp} = 0.85$ Mm^{-1} sr^{-1} (see Fig. 5), we derived an ash mass concentration $M_{ash} = (270 \pm 70)$ μg m^{-3} by assuming that diameter 10 μm ash particles dominate the ash mass concentration with an ash mass density of 2600 kg m^{-3}, as reported by the Global Volcanism Program (http://www.volcano.si.edu). The retrieved value at 4.2 km altitude is twice larger than values usually observed at ground level during strong pollution events (Miffre et al., 2010) and lies in the range of FLEXPART ash mass concentrations (Fig. 4, top). The uncertainty on M_{ash} depends on the scattering cross-section calculation and on the S-ratio. The ash mass density adds a systematic error of 25%. When volcanic particles mix into the PBL on April 18th, parallel backscattering enhancement relies on the volcanic ash particles intrusion, as shown by FLEXPART, and on possible sulfate hygroscopic growth (see next sections). On April 19th, $\beta_{p,//}$-values decrease caused both by the reduced volcanic activity after the initial eruption and less direct transport to the measurement site. An interesting feature occurs between 3 and 5 km altitude where, in agreement with back-trajectories, new ash layers are simulated by FLEXPART in high mass concentrations. By

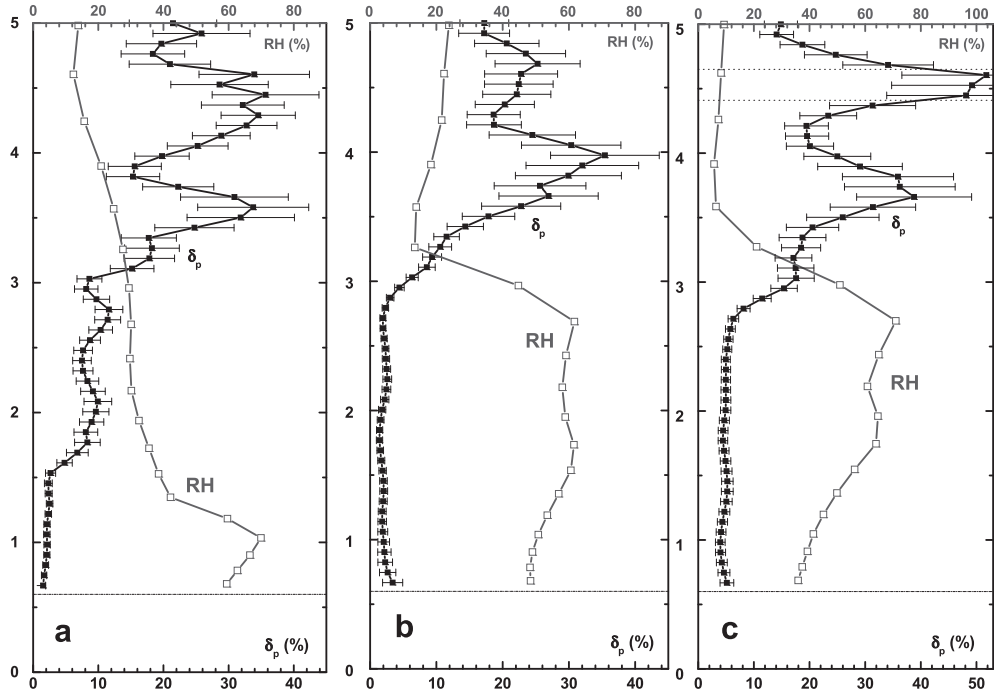

Fig. 6. Vertical profiles of particle UV-depolarization ratio δ_p and relative humidity (RH) as a function of altitude at specific times: (a) April 17th at 12 h UTC; (b) April 19th at 0 h UTC, (c) April 19th at 19 h UTC.

the same time, low $\beta_{p,//}$-values are observed on Fig. 4, dedicated to scattering on the parallel polarization channel. As shown in the next paragraph, it is necessary to include Fig. 6-depolarization profiles, to further interpret the comparison of the measurements to the FLEXPART ash dispersion model.

4.2. Optical properties of volcanic particles (scattering and depolarization)

The Lidar profiles exhibit a high variability in time and space, for both scattering (Figs. 4 and 5) and depolarization (Figs. 5 and 6). It can be seen that depolarization ratios are not related to backscattering coefficients in a simple way, as noticed by Winker and Osborn for stratospheric studies (1992). On April 17th at 12 h, both scattering (Fig. 4, bottom) and depolarization (Fig. 6a) are quite high in the volcanic layer at 4.2 km altitude where ash particles are present in high mass concentration, as confirmed by FLEXPART, and efficiently depolarize laser light. On April 19th at 00 h, the depolarization profile (Fig. 6b) reveals low values for altitudes below 3 km with high particle scattering (Fig. 4, bottom), while on April 19th at 19 h, there are two volcanic layers of a few hundred meters depth between 3.5 and 5 km altitude, corresponding to poorly scattering (Fig. 4, bottom) but strongly depolarizing (Fig. 6c) particles. The highest 4.5 km-layer (Fig. 6c-dashed lines delimitation), which corresponds to the observed highest depolarization value over the three profiles in Fig. 6, can be attributed to volcanic ash particles in agreement with Munoz's et al. (2004) value of 44% (see Section 2.3) within our error bar. The observed ash particles preserve their intrinsic optical depolarization property, even after long-range advection. This remark may not be generalized as a general property. For this, history on the air parcel chemistry should be available. Within our error bars, the lower layer at 3.7 km on Fig. 6c, which exhibits slightly lower depolarization, is not only containing ash particles. Inside the volcanic cloud, the lower depolarization values, observed on each of the three profiles in Fig. 6, can be attributed to volcanic layers composed of non spherical ash particles and spherical particles, most likely hydrated sulfates particles. As sulfate particles are hygroscopic, they scatter light more efficiently when RH-values increase (Li et al., 2001). Water uptake is much more efficient on sulfate particles than on ash particles (Delmelle et al., 2007). From the δ_p-definition, it follows that δ_p will decrease, as $\beta_{p,//}$ increases, as seen on profiles (b) and (c) in Fig. 6 for altitudes below 3 km. In this altitude range, we still observe 5%-depolarization on profile (c), that we relate to remaining fine ash particles (simulated by FLEXPART) and fine hydrated spherical particles.

4.3. Ash concentrations, partitioning between spherical and non spherical particles

The assumed mixture of ash and sulfate particles (Mather et al., 2003; Schumann et al., 2010) is further confirmed by comparing our data with CALIPSO satellite measurements (http://www-calipso.larc.nasa.gov/products/lidar). When CALIPSO satellite passed over Lyon (17th April, 2 h UTC, volcanic cloud at 6 km-altitude), we estimated a backscatter Ångstrom exponent of 1.02, by assuming a power law dependence of the particle backscatter coefficient with the 355 (Lyon Lidar) and 532 nm (CALIPSO) laser wavelengths. As shown by Sasano and Browell (1989), the Ångstrom exponent is related to the chemical composition of the volcanic particles but primarily depends on their size. Our value indicates that after long-range advection, there is no evidence that scattering from ash particles is dominant. Under the assumptions of a 44%-ash depolarization ratio and a negligible depolarization ratio for hydrated sulfates particles, we evaluated the ash particles backscattering coefficient from our (β_p, δ_p) measurements. These assumptions may be violated if ash particles induce ice-cloud nucleation (Durant et al., 2008) but our meteorological data show that these conditions are not fulfilled within our altitude range. We then estimated the particle concentration number N_{ash} of ash particles, by using computed backscattering cross-sections (see Section 2.3). The N_{ash}-uncertainty depends on the ash particles

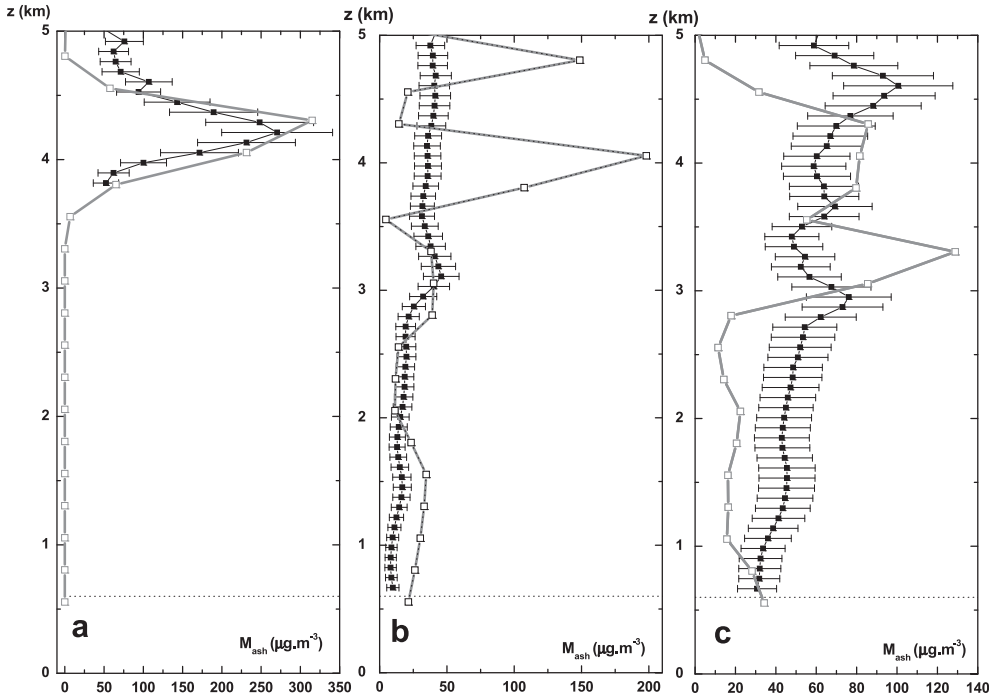

Fig. 7. Vertical profiles of volcanic ash mass concentration for each depolarization profile: (a) April 17th at 12 h UTC; (b) April 19th at 0 h UTC, (c) April 19th at 19h UTC. Fig. 4-ash mass concentrations vertical profiles (gray empty squares) are added for quantitative comparison.

backscattering coefficient which is range-dependent and on the optical computation (20 %-error). Ash mass concentrations M_{ash} can be evaluated from N_{ash} by using the number-to-mass conversion factor of 1.08×10^{-2} µg part^{-1}. Vertical profiles of M_{ash} are displayed in Fig. 7. All retrieved mass concentrations are well below the limit value of 2000 µg m^{-3} chosen for airport closures. In the PBL, the low ash concentration is comparable with 10–40 µg m^{-3} PM10 concentration measured at ground level in urban polluted areas (Miffre et al., 2010). The highest M_{ash}-value, (270 ± 70) µg m^{-3}, is observed on April 17th at 12 h (Fig. 7a) in the volcanic layer at 4–4.5 km altitude (M_{ash}-values are not evaluated under 4 km as air masses do not originate from the volcano), in excellent agreement with FLEXPART ash simulation. Profiles (7b) and (7c) exhibit lower M_{ash}-values for the new ash intrusions, and when particles mix into the low troposphere, M_{ash}-values are even lower, in agreement with FLEXPART. The observed discrepancy above 3 km between FLEXPART and Lidar ash mass concentrations may be due to the air masses hanging around in Europe moving back and forth as suggested by Fig. 2 back-trajectories; rain further complicates the situation. The ash mass concentration profile follows the depolarization profile only for low RH-values (around 10%). On April 19th at 19 h, when δ_p decreases (Fig. 6c) and RH increases, as between 3.5 and 3 km, this is not a clear indication that the ash particles concentration is decreasing (Fig. 7c). This δ_p-decrease relies on the hygroscopic growth of spherical particles. The retrieved ash concentrations should therefore be carefully compared with optical counter measurements (Schumann et al., 2010).

Complementary optical scattering of hydrated sulfates particles (Section 2.3) leads to the evaluation of the (concentration) number ratio $NR = N_s/N_{ns}$ between spherical (N_s) and non spherical (N_{ns}) particles. On Fig. 6c, RH-values strongly vary, at 4 km, RH = 10% and NR is equal to 1000, whereas at 2.7 km, RH = 70% and NR = 3000. These two values are different as these volcanic air masses are different. The air mass at 2.7 km has a higher NR-value due to lower ash particle concentrations and higher concentrations of spherical hydrated sulfate particles. Despite a large uncertainty, we can in this way evaluate the mixing number ratio between hydrated particles and solid particles, under the assumption that ash particles are not sufficiently hygroscopic (Delmelle et al., 2007). This assumption can be questioned, in which case surface reactions may occur. However, the efficiency of this process is yet unknown, and hence difficult to estimate. Moreover, a recent publication from Sipilä et al. (2010) shows that, under these low tropospheric conditions, sulfuric acid nucleation can compete this surface process.

5. Conclusions

In this contribution, an UV-polarization Lidar has been used to measure, with high sensitivity and accuracy, the optical properties of highly diluted and aged volcanic ash particles, after more than 2600 km of advection. The FLEXPART particle dispersion model has been applied to simulate the volcanic ash dispersion from Iceland to South West Europe, at the border of the air traffic closure area. Both methodologies nicely agree and show the transport of volcanic particles into the low troposphere. Moreover, a microphysical analysis has been made by using optical scattering calculation and laboratory measurements from volcanic ash particle samples (Munoz et al., 2004). Fine remaining ash particles, which exhibit high UV-depolarization ratios, still have an irregular shape after long-range transport, even at low ash concentrations. Such a high depolarization may lead to non-negligible effects on atmospheric radiative transfer and may affect satellite remote sensing measurements. Our methodology, based on high sensitivity depolarization measurements, leads to an estimation of number and mass ash concentrations. The inferred ash mass concentration does not exceed typical urban PM10 concentrations. In addition to ash particles, the environmental effect of the Eyjafjalla volcanic particles may be due to sulfate particles, whose concentration number has been also estimated from our methodology. We observe a strong amplification of the atmospheric light scattering in layers

with higher relative humidity values, such as in the lower atmosphere. In this case, optical backscattering coefficient from sulfate particles may exceed the optical backscattering coefficient from ash particles by a factor 15, whereby the number density ratios between ash and sulfates are 3000. This estimate is based on our analysis of both scattering and depolarization measurements. As an outlook, this study shows that ash particles are low-number concentrated and their large surface may enhance chemical reactions involved in the atmosphere, as pointed out by Mather et al. (2003), Delmelle et al. (2007) and Schumann (2010).

Acknowledgments

We would like to thank O. Munoz for fruitfull discussions on scattering properties on volcanic ash particles, region Rhône-Alpes, which partly funded this work. N.I.K. and A.S. were supported by the European Space Agency (ESA) in the framework of the SAVAA project.

References

Ackermann, J., 1998. The extinction-to-backscatter ratio of tropospheric aerosol: a numerical study. Journ. Atm. Ocean. Tech. 15, 1043–1050.
Allen, A.G., et al., 2002. Primary sulfate aerosol and associated emissions from Masaya Volcano, Nicaragua. Journ. Geophys. Res. A 107, D23.
Alvarez, J.M., et al., 2006. Calibration technique for polarization-sensitive Lidars. J. Atm. Ocean. Tech. 23, 683–699.
Ansmann, A., et al., 2010. The 16 April 2010 major volcanic ash plume over central Europe: EARLINET lidar and AERONET photometer observations at Leipzig and Munich, Germany. Geophys. Res. Lett. 37, L13810.
Böckmann, C., et al., 2005. Aerosol backscattering algorithms. Appl. Opt. 43 (4), 977–989.
Delmelle, P., et al., 2007. Gas/aerosol–ash interaction in volcanic clouds: new insights from surface analyses of fine ash particles. Earth Planet. Sci. Lett. 259 (1–2), 159–170.
Durant, A.J., et al., 2008. Ice nucleation and overseeding of ice in volcanic clouds. Journ. Geophys. Res. 113, D09206.
Eckhardt, S., et al., 2008. Estimation of the vertical profile of sulfur dioxide injection into the atmosphere by a volcanic eruption using satellite column measurements and inverse transport modeling. Atmos. Chem. Phys. 8, 3881–3897.
Halmer, M.M., et al., 2002. The annual volcanic gas input into the atmosphere. J. Volc. Geotherm. Res. 115, 511–528.
Klett, J.D., 1985. Lidar inversion with variable backscatter/extinction ratios. Appl. Opt. 24, 1638–1643.
Krotkov, N.A., et al., 1997. Ultraviolet optical model of volcanic clouds for remote sensing of ash and sulfate dioxyde. Journ. Geophys. Res. 102 (D18), 21891–21904.
Li, J., et al., 2001. Parameterization of the optical properties of sulfate aerosols. Journ. Atm. Sci. 58, 193–209.
Mather, T.A., Pyle, D.M., Oppenheimer, C., 2003. Tropospheric volcanic aerosol, volcanism and the earth's atmosphere. Geophys. Monogr. 139, 189–212. 10.129/139GM12.
Miffre, A., et al., 2010. Aerosol load study in urban area by Lidar and numerical model. Atm. Env 44, 1152–1161.
Mishchenko, M.I., 2002. Scattering, Absorption and Emission of Light by Small Particles, third ed. Cambridge University Press, UK.
Munoz, O., et al., 2004. Scattering matrices of volcanic ash particles of Mount St Helens, Redoubt, and Mount Spurr volcanoes. J. Geo. Res. 109, D16201.
Murayama, T., Masonis, S.J., Redemann, J., et al., 2003. An intercomparison of Lidar derived aerosol optical properties with airborne measurements near Tokyo during ACE-Asia. J. Geo. Res. 108, D238651.
Ovadnevaite, J., et al., 2009. Volcanic sulfate and arctic dust plumes over the North Atlantic Ocean. Atm. Env. 43, 4968–4974.
Prata, A.J., Tupper, A., 2009. Aviation hazards from volcanoes: the state of the science. Nat. Hazards 51 (No. 2), 239–244.
Ramaswamy, V., et al., 2001. Stratospheric temperature trends: observations and model simulations. Rev. Geophys. 39 (1), 71–122.
Robock, A., 2000. Volcanic eruptions and climate. Rev. Geophys. 38, 191–219.
Sasano, Y., Browell, E.V., 1989. Light scattering characteristic of various aerosol types derived from multiple wavelength lidar observations. Appl. Opt. 28, 1670–1679.
Sassen, K., et al., 2007. Volcanic ash plume identification using polarization lidar: augustine eruption, Alaska. Geophys. Rev. Lett. 34, L08803.
Schumann, U., et al., 2010. Airborne observations of the Eyjafjalla volcano ash cloud over Europe during air space closure in April and May 2010. Atm. Chem. Phys. Discuss. 10, 22131–22218.
Sipilä, M., et al., 2010. The role of sulfuric acid in atmospheric nucleation. Science 327, 1243–1246.
Stohl, A., et al., 1995. Interpolation errors in wind fields as a function of spatial and temporal resolution and their impact on different types of kinematic trajectories. J. Appl. Meteor 34, 2149–2165.
Stohl, A., et al., 2005. Technical note: the Lagrangian particle dispersion model, FLEXPART version 6. Atmos. Chem. Phys. 5, 2461–2474.
Stohl, A., Prata, A. J., Eckhardt, S., Clarisse, L., Durant, A., Henne, S., Kristiansen, N. I., Minikin, A., Schumann, U., Seibert, P., Stebel, K., Thomas, H. E., Thorsteinsson, T., Tørseth, K., and Weinzierl, B., 2011. Determination of time- and height-resolved volcanic ash emissions for quantitative ash dispersion modeling: the 2010 Eyjafjallajökull eruption, Atmos. Chem. Phys. Discuss. 11, 5541–5588, doi:10.5194/acpd-11-5541-2011.
Wang, X., et al., 2008. Volcanic dust characterization by EARLINET during Etna's eruptions in 2001-2002. Atm. Env. 42, 893–905.
Winker, D.M., Osborn, M.T., 1992. Preliminary analysis of observations of the Pinatubo volcanic cloud with a polarization-sensitive lidar. Geophys. Res. Lett. 19, 171–174.
Witham, C.S., et al., 2007. Comparison of VAAC atmospheric dispersion models using the 1 November 2004 Grimsvötn eruption. Meteorol. Appl. 14, 27–38.